

**Tectonic and climatic controls on rift escarpments:  
Erosion and flexural rebound of the Dhofar passive margin  
(Gulf of Aden, Oman)**

C. Petit (1)\*, M. Fournier (1), and Y. Gunnell (2)

Revised version

*Submitted to : Journal of Geophysical Research, Solid Earth*

\*Corresponding author (1): Laboratoire de Tectonique, CNRS UMR 7072, Université de Paris VI, Tour 46-00 E2, Boite 129, 4 Place Jussieu, 75252 PARIS CEDEX 05, France.  
Tel : +33 1 44 27 38 71. [carole.petit@lgs.jussieu.fr](mailto:carole.petit@lgs.jussieu.fr)

(2): Laboratoire de Géographie Physique, CNRS UMR 8591, Université de Paris VII, Boîte 7001, 2 Place Jussieu, 75251 PARIS cedex 05, France. Tel : +33 1 44 27 81 39

## **Abstract.**

We investigate the respective roles of climatic parameters and the flexural rigidity of the lithosphere in the erosion history and behavior of two adjacent rift escarpments along the northern coast of the Gulf of Aden, in Oman. At this 25 My-old passive margin, we define a Type 1 scarp, which is high, sharp-crested and has retreated 25–30 km inland from its master fault, and a Type 2 scarp, which exhibits a more rounded profile, lower relief, and still coincides with its mapped normal fault trace. Since about 15 Ma, the margin has been seasonally affected by monsoon precipitation but with contrasting effects at the Type 1 and Type 2 escarpments depending on the position of the Intertropical Convergence Zone in the geologic past: during peak monsoon conditions, both scarps experienced heavy rainfall and runoff, whereas during monsoon-starved conditions (such as today), the Type 2 scarp experienced a foggy, moist climate while the Type 1 scarp remained much drier. In order to assess the relative effects of climate and flexural parameters on the present-day morphology of the Dhofar margin, we present one-dimensional numerical models of erosion and flexure along two profiles representative of the Type 1 and Type 2 scarps. Unlike most surface process models previously published, where present-day topography is the only criterion by which to evaluate the quality of model outputs, model behavior here is additionally constrained by independent estimates of denudation provided by geological cross-sections, well defined fault traces, and other stratigraphic markers. The best-fitting models indicate that the Type 1 escarpment formed under relatively arid climatic conditions and was affected by significant erosion, recession and flexural uplift due to a low (7 km) effective elastic thickness. In contrast, the morphology of the Type 2 fault scarp was smoothed by a more humid climate, but a high effective elastic thickness ( $\geq 15$  km) prevented it from uplifting or receding. In addition, we show that the sedimentary load acting at the foot of the escarpments exerts significant influence on their morphological evolution, though this parameter is often neglected in other scarp evolution models.

# 1 Introduction

Rifted continental margins often exhibit high topographic escarpments even where continental rifting is known to have ceased several tens of millions years ago [e.g., *Gilchrist and Summerfield*, 1990; *Gilchrist et al.*, 1994; *van der Beek et al.*, 1995]. Thus, whereas initial relief, referred to as a rift shoulder, is caused by rift tectonics and flexural rebound of the extended lithosphere [e.g., *Weissel and Karner*, 1989], the persistence of an evolving escarpment through time is usually attributed to a combination of erosional processes and flexural response of the lithosphere to the corresponding redistribution of mass across the landscape. This has been demonstrated in a range of numerical surface process models, or SPMs [e.g., *Gilchrist et al.*, 1994; *Kooi and Beaumont*, 1994; *ten Brink and Stern*, 1992; *van der Beek et al.*, 2002]. However, different modeling scenarios involving different sets of parameters such as initial topography (usually an arbitrary input), erosion constants, and flexural response can produce topographic landscapes that nevertheless share similar appearances [*Gunnell and Fleitout*, 1998]. Equifinality is therefore a challenge to SPMs because even though the synthetic landscapes generated by them may be successful in mimicking present-day topography, it remains difficult to determine whether the natural landscape and the SPM have the same landscape development histories [*Gilchrist et al.*, 1994]. When used as a tool to constrain lithospheric rigidity and dominant erosion processes, the quality of long-term landscape development models at rift escarpments is potentially improved when the observed topography is combined with other independent quantitative data, such as low-temperature thermochronology [*Gunnell et al.*, in review]. Most accurate of all, however, and in addition to present-day topography, structural and tectonic markers such as faults and major stratigraphic unconformities, whose geometries before erosion and flexural response can be determined, represent ideal constraints on the amount of denudation and uplift.

Such constraints are rarely available, but the northern margin of the Gulf of Aden, in the Dhofar region of Oman, is particularly well suited to address this problem: it is a ~25 My old passive margin structured by en-échelon normal faults and displaying a contrasted topography, with spectacular south-facing escarpments [e.g., *Fournier et al.*, 2004]. Given that the margin is young and devoid of volcanic deposits, that the position of major normal faults is well known, and that the geology consists mainly of pre-rift marine deposits, it is relatively easy to reconstruct relief development and evaluate erosion depths since sedimentation ended and uplift occurred. An additional aspect, critical to the SPM presented

in this paper, is that the stratigraphy is marked by a regional unconformity between the basement and the overlying sediment sequence. The unconformity has been exposed by erosion at the scarp face and connects to several outlying buttes located near the coast. Finally, strengthening of the summer monsoon on the eastern part of the margin ca. 15 My ago is hypothesized to have had a critical influence on the mechanisms and rates of relief development [Prell *et al.*, 1990].

In this paper, we present two one-dimensional (1-D) SPMs of rift escarpment erosion and flexural rebound on two NW–SE profiles crossing the Dhofar margin. We evidence large spatial variations in the lithospheric rigidity, as well as an important influence of the summer monsoon flow on escarpment morphology. Constraints on the amount of denudation and on the pre-erosive topography are provided by geologic cross-sections.

## 2 Geologic setting

### 2.1 Rift history and geologic structure

The opening of the Gulf of Aden is presently accommodated by oblique sea-floor spreading along the Sheba ridge (Fig. 1). The onset of oceanic spreading occurred at ca. 18 Ma [d'Acremont *et al.*, 2004; Leroy *et al.*, 2004] and seafloor spreading currently occurs along the mid-oceanic Sheba Ridge at a full rate of 22 mm/year along N25°E at the longitude of Dhofar [Fournier *et al.*, 2001]. It was preceded by rifting of the continental lithosphere, which started in the Oligocene epoch and continued until the early Miocene [Roger *et al.*, 1989; Hugues, 1991; Watchorn *et al.*, 1998]. Two simultaneous directions of extension prevailed during rifting: (1) a N20°E direction, parallel to the direction of opening of the Gulf of Aden; and (2) a N150°E direction, perpendicular to the N75°E mean trend of the Gulf of Aden [Lepvrier *et al.*, 2002; Huchon and Khanbari, 2003; Fournier *et al.*, 2004; Bellahsen *et al.*, 2006]. Rifting created a series of grabens bounded by N70°E to N110°E normal faults (Fig. 2).

In Dhofar, the margin is dominated by a gently dipping plateau tilted a few degrees towards the north, made up of mainly Eocene platform carbonates. The plateau is bounded to the south by the south-facing escarpments of Jabal al Qamar, Jabal Qara and Jabal Samhan (Fig. 2), which rise up to 1800 m and define the northern shoulder of the rift. The Ashawq and Hasik main grabens and the Haluf and Sala'Afan minor grabens occur inboard of the main escarpment (Fig. 2). The two main grabens present an axial dip toward the east. A carbonate succession up to 1000 m thick is exposed [Platel and Roger, 1989; Roger *et al.*, 1989]. The

Cenozoic series includes the pre-rift, syn-rift and post-rift stages of deposition, respectively. The pre-rift sediments of Eocene age rest unconformably upon Cretaceous strata, which in turn overlie the Proterozoic [ $\sim 800$  My; *Mercolli et al.*, 2006] basement. Except for the low-angle unconformity between Cretaceous and Eocene sediments, the remarkably constant thickness of the sedimentary sequence suggests that it was deposited on a flat surface.

The pre-rift series consist mainly of massive limestones typical of shallow-water conditions. The syn-rift sediments consist of lacustrine limestone at the base, overlain by platform limestone, which passes laterally at top to the overlying, chalky calci-turbiditic deposits of the late Oligocene to early Miocene [*Platel et al.*, 1992]. These sediments are characterized by slope deposits including mega-breccia, debris flows, and olistolithic material transported from the adjoining shelf and correspond to deeper depositional environments. The post-rift sequence is restricted to a narrow zone following the coastline, and is made of proximal carbonate and conglomeratic marine deposits. The change in the type of sedimentation expressed in the facies of the post-rift sequence, from open to shallow marine carbonate and detritic deposits, was caused by the emergence and erosion of southern Dhofar. Sedimentary conditions were at that time very similar to the present-day environments.

Thus, the continental rifting in Dhofar can be dated between the Oligocene and the end of the Lower Miocene, i.e. between 34 and 18 Ma, with a peak phase starting at  $\sim 25$  Ma with the occurrence of slope deposits. Emergence of southern Dhofar was achieved shortly after the rifting stage; however, the youngest sediments outcropping north of Jabal Qara and Jabal Samhan are of early Oligocene age, suggesting that these rift escarpments were already emerged during most of the rifting period while deep basins were developing.

## **2.2 Monsoon precipitation, drainage and erosional potential in Dhofar**

The drainage network of Dhofar falls into three domains (Fig. 3A). North of the main coastal topographic escarpment and drainage divide, rivers flow towards the north over the gentle slope of the Arabian plateau. Whereas river channels appear strongly incised close to the top of the escarpment, stream power seems to decrease very rapidly north of it as indicated by a lower degree of fluvial incision (Fig. 3A). South of the main drainage divide, short streams run across the southern slope of the escarpment, perpendicular to its strike. Both drainage systems appear controlled by the general morphology of the Dhofar margin. Along the coast, some rivers flow towards the east or northeast following the main trend of marginal grabens. This indicates a control on the drainage geometry by tectonics (Fig. 3A).

The northern margin of the Gulf of Aden is under the influence of southwest monsoon winds from June to September [Jung *et al.*, 2002]. These winds are responsible for seasonal upwelling in the Indian Ocean along the coast of Oman. This is recorded in the offshore sedimentary sequence, and Ocean Drilling Program (ODP) cores in the Arabian Sea have provided an estimate of the onset of summer monsoon activity at ca. 15 Ma on that basis [Prell *et al.*, 1990]. Before that time, the entire Dhofar margin was semiarid. Landsat images of Dhofar during the summer monsoon season evidence a spatially variable impact of moist monsoon air along the strike of the margin (Fig. 3B): whereas in the western two thirds, natural vegetation growth, correlated with green patches on the Landsat image, reflects a transient rise in humidity, the eastern third remains dry. Two main factors explain aridity in Dhofar. Firstly, on average, monsoon winds are parallel to the Oman margin between Hadhramaut (in Yemen) and Pakistan, so despite their relief of 1.5–2 km, the rift escarpments do not represent perpendicular obstacles likely to generate precipitation by forced orographic ascent. Secondly, the cloud cover during the monsoon does not rise higher than 1.5 km a.s.l. because of a temperature inversion created by the stratification between mid-tropospheric northwesterly winds and the low-level southwest monsoon wind system [Fig. 4; Sirocko *et al.*, 1991]. This inversion inhibits the deep convection required for high-energy precipitation. Instead, precipitation occurs as drizzle because the cold upwellings nevertheless allow dewpoint to be reached. Summer precipitation rarely exceeds daily averages of 5 mm but still remains among the highest fog precipitation totals in the world [Sale, 1980]. A vertical humidity gradient is observed, with precipitation maxima (0.4–0.5 m·yr<sup>-1</sup>) occurring at the Salalah escarpment (known to botanists as the Oman ‘fog oasis’), and minima at the coast (0.1 m·yr<sup>-1</sup> at Salalah).

The capacity for fog to generate runoff and erode is limited. Intuitively, this would suggest that the escarpments have been largely stagnant for 15 My or more despite the intensification of the monsoon as detected in the marine geologic record [Prell *et al.*, 1990]. However, this view overlooks two key elements: firstly, at timescales corresponding to the Quaternary and probably longer, the position of the intertropical convergence zone (ITCZ) has fluctuated in latitude. As a result, monsoon airflow has penetrated deeper into the Arabian continent, thus striking the escarpment perpendicularly (Fig. 4) and generating summer orographic precipitation more typical of monsoon settings at passive margin escarpments [e.g., Gunnell, 1998]. During such times, the thermal inversion was also situated at higher altitudes and allowed deeper tropospheric convection. The last time this has been documented to occur was the early Holocene, with evidence from cave stalagmites near Salalah

[Fleitmann *et al.*, 2003]. Such fluctuations are shown to correlate with temperature variations in the North Atlantic (Greenland ice cores, etc.), and suggest that the cumulative impact of ITCZ fluctuations is driven by global orbital cycles and has been much larger on the landscape of Dhofar than suggested by current conditions. The image of the Dhofar escarpment as just a fog oasis is therefore a transient one.

Secondly, even in times similar to present-day monsoon-starved conditions, the geomorphic impact of pre-monsoon precipitation cannot be overlooked. Southern Dhofar is reputed for cyclonic storms in May–June and sometimes in autumn, with high runoff and severe flooding (e.g. May 10, 2002 in Salalah). The magnitude of infrequent but high-intensity events in sparsely vegetated terrains is known to have higher cumulative effects on landscape and sediment flux than high-frequency but low-magnitude (e.g. fog) climatic events that are sufficient to green the land (cf. Fig. 3B) but not to erode bedrock or even transport regolith. Instead, humid climates promote weathering and the rounding of hillslope profiles [Kooi and Beaumont, 1994]. Finally, we note that in Dhofar, the abrupt changes from humid to arid areas along the escarpment strike correspond to changes in escarpment direction (Figs. 2 and 3B), suggesting a possible influence of relief geometry on the strength of monsoon precipitation. This could also explain why the Salalah hinterland, which forms a re-entrant with respect to the coast-parallel wind stream, currently receives comparatively more precipitation than the eastern escarpment (Fig. 3B).

## **2.3 Two distinct escarpment morphologies**

### **2.3.1 Type 1 scarp(s)**

The Dhofar margin displays a succession of contrasting escarpment morphologies along its strike (Figs. 5 and 6). East of longitude 54.7°E, the margin is fringed by a steep, 1500 m-high escarpment (Jabal Samhan) located about 25 km inland and separating the northward-sloping plateau from a dissected piedmont to the south (Fig. 5A). The present-day topographic escarpment is not bounded by a master normal fault [Platel *et al.*, 1992], and thus appears to be of purely erosional origin. The location of the closest normal fault offshore suggests that this rift escarpment has retreated 25–30 km inland with respect to its original syn-rift position. The present-day drainage divide coincides with the top of the escarpment. A closer view of the escarpment crest shows decapitation and capture of north-flowing channels by those flowing southwards, which indicates that the drainage divide has migrated inland with the escarpment crest (Fig. 5B). Surface geology reveals that the dissected piedmont consists of

Proterozoic basement rocks [Mercolli *et al.*, 2006], whereas the plateau and some buttes located at the coast are topped by a thick (500–1000 m) Cretaceous and Eocene sedimentary cover [Platel *et al.*, 1992]. The unconformity between the basement and sediments outcrops ~400 m beneath the top of the escarpment and close to sea level where the buttes occur (Fig. 5C). As there is no evidence of a progressive onlap of the sedimentary sequence on a preexisting topography, we can conclude that the unconformity between basement and sediments was horizontal before rifting. This indicates that the entire sedimentary sequence, as well as a variable thickness of crystalline basement, has been eroded between the shoreline and the present-day escarpment. The drop in altitude of the unconformity between the escarpment and the buttes suggests that erosion has been associated with flexural uplift of the margin. Critical to this configuration is that the buttes are not defined by major extensional faults [Platel *et al.*, 1992; Mercolli *et al.*, 2006], although we cannot completely rule out the existence of undetected small-scale normal faults in the Proterozoic basement [Mercolli *et al.*, 2006].

In summary, this escarpment, which we name “Type 1 scarp”, exhibits a steep topographic slope and is disconnected from its original master fault. Preserved steep slopes and high topography associated with scarp retreat are likely to result from the combination of erosion and flexural rebound [e.g., Gilchrist and Summerfield, 1990]. We assume that, prior to erosion, the sedimentary cover was capped by the youngest, conformable Eocene formation outcropping on the plateau (represented in light grey on Fig. 5C). Denudation estimates inferred from the geologic cross-section range between 0–50 m at about 100 km north of the escarpment where the youngest Eocene rocks occur, to a maximum value of 1700–1800 m at its foot (Fig. 5C). These values are in agreement with denudation estimates obtained by combined AFT and (U–Th)/He analysis, which yielded an average coast-to-scarp denudation depth of 1750 m [Gunnell *et al.*, in review]. The geologic cross-section shows that the sedimentary cover of the plateau, which was deposited horizontally, now displays a concave-up shape with steepening dips close to the escarpment crest. Interpolation of the basal unconformity between the scarp and the unfaulted coastal buttes defines an anticlinal structure, which reflects the flexural uplift due to erosion. Reconstruction of the pre-erosive topography is performed by unfolding the basement/sediment unconformity in order to obtain a monoclinical plateau with a dip angle similar to those observed in the northern part of the profile. The reconstructed cross-section suggests that, prior to erosion, the rift escarpment was ~1500 m high at the master fault (Fig. 5C).

### 2.3.2 Type 2 scarp(s)

West of 54.7°E, the plateau edge changes laterally to a smooth, ~1000 m-high escarpment (Jabal Qara) facing the flat, low-lying sedimentary plain of Salalah (Fig. 6A). The scarp-foot slope break coincides with the position of the master normal fault that has been controlling basin subsidence and the initial escarpment uplift since rifting. Whereas scarp-foot retreat from the original fault line has been minimal, the present-day drainage divide is located ~20 km inboard of the main escarpment (Figs. 3A and 6). Streams flowing towards the south rapidly lose power when reaching the Salalah plain and eroded sediments are deposited onshore in the basin. Mapped Quaternary slope deposits at the foot of the escarpment mask the normal fault trace (Fig. 6B). Unlike the adjacent Type 1 scarp, basement rock outcrops are absent, indicating that depths of erosion have remained comparatively limited. However, some outcrops of Cretaceous sediments suggest that the unconformity lies at shallow depths close to the scarp foot (Fig. 6C). We define here a “Type 2 scarp”, which displays a rounded slope profile with low relief, comparatively low topographic slope angles, and no significant retreat from its master fault. Unlike the Type 1 scarp, erosion has degraded the initial topography and lowered the slopes, but flexural rebound does not seem to have played a major role because the signs of uplift detected at the Type 1 scarp (see section 2.3.1) are negligible (flat-lying strata are clearly visible on Fig. 6B). The reconstruction of the pre-erosive topography is complicated by the presence of the small Haluf graben inboard of the escarpment. For simplicity, we disregard the topography related to this second-order tectonic feature. Denudation estimates from the geological cross-section are ~1100 m close to the normal fault and decrease rapidly to a mean value of 250–300 m north of it (Fig. 6). The initial topography of this escarpment is reconstructed as a north-dipping plateau parallel to the initial topography defined for the Type 1 scarp (Fig. 6C). In this case, the initial altitude of the rift escarpment is ~1100 m.

In previous studies on the evolution of passive margin topography, Type 1 and Type 2 escarpments have been recognized and associated with two contrasting phenomena named “escarpment retreat” and “plateau degradation”, respectively, by *van der Beek et al.* [2002] after conceptual models formulated by a range of previous authors. The occurrence of one or the other of these processes is thought to depend primarily on the pre-existence (plateau degradation) or not (escarpment retreat) of a drainage divide located inboard of the main escarpment. However, the restored geologic cross-section for the Type 2 scarp does not provide unequivocal evidence for an antecedent drainage network (Fig. 6C). Instead, the present-day drainage divide coincides, on the geologic cross-section, with a small, narrow

graben (the Haluf graben) in the footwall upland, and it is unlikely that such a depressed structure would have produced a topographic high prior to the post-rift period. In summary, there is no clear explanation for the rapid lateral change from Type 1 to Type 2 escarpments along the strike of the Dhofar passive margin. Here, we consider climatic change in both space and time, initial topography and lithospheric elastic thickness ( $T_e$ ) as being key to any model seeking to understand what controls the contrasting morphologies of the adjacent Type 1 and Type 2 rifted margin escarpments of southern Dhofar.

### **3 One-dimensional model of scarp denudation and flexure**

We use a 1-D version of the SPM described by *Kooi and Beaumont* [1994] to simulate erosion, retreat and subsequent uplift of Type 1 and Type 2 rift escarpments. This SPM was especially designed for modeling the large-scale evolution of rifted margins. In one-dimensional models, “surface” processes are necessarily restricted to the profile dimension, with the hypothesis that mass transfers in the perpendicular dimension are negligible. Moreover, flexure is also supposed to occur dominantly in the direction of the profile. Given the dominant NW-SE direction of topographic slopes and river channels, the use of one-dimensional models appears a reasonable approximation to the Dhofar setting. The model iteratively computes the denudation due to short- and long-range transport processes, and the resulting flexural rebound of the lithosphere. In the next sub-section we briefly summarize the general aspects of this model, following *Kooi and Beaumont* [1994] and *Gilchrist et al.* [1994].

We use as constraints (i) the observed topography, extracted from a digital elevation model [SRTM; *Rodriguez et al.*, 2005] as strike-perpendicular line profiles; (ii) the observed form of the basal unconformity in the stratigraphy; and (iii) the estimated amounts of erosion (see previous sections and Figs. 5 and 6) derived from stratigraphic sections and low-temperature thermochronologic data [*Gunnell et al.*, in review]. The model consists of a 1-D grid with spacing between grid points of 1 km and a total length of 1000 km. The time duration of the model is 25 Ma, which corresponds to an average estimate of the independently established erosion period (see section 2.1).

#### **3.1 Short- and long-range transport processes**

In the absence of active uplift, short-range transport processes are represented as slow and continuous diffusive processes related to topographic curvature, i.e. the second derivative of

elevation  $h$ . They tend to smooth and flatten topography over time, and they obey a classical diffusion law:

$$\frac{dh}{dt} = K_d \frac{d^2h}{dx^2} \quad (1)$$

where  $dh/dt$  is the denudation rate,  $\frac{d^2h}{dx^2}$  is local slope curvature and  $K_d$  is the diffusivity coefficient. In the following models, we assume that  $K_d$  is constant, thus neglecting the effect of lateral and/or vertical lithological contrasts. This is a reasonable assumption given that the 1 km-thick sediment package overlying the basement is essentially limestone. Given the limestone bedrock, we also disregard processes that cause landsliding and involve threshold slope angles. The result is that scarp morphology becomes homogeneously smoothed over time.

Long-range fluvial transport depends on the ability of rivers to carry sediments away from the initial scarp. We use a simple linear relationship where the equilibrium sediment flux  $q_f^{eqb}$  is:

$$q_f^{eqb} = -K_f q_r \frac{dh}{dx} \quad (2)$$

where  $\frac{dh}{dx}$  is the local slope,  $K_f$  is a transport coefficient and  $q_r$  is the local river discharge per unit width. Since the model is one-dimensional, river width is assumed (as also in most 2-D models) to be constant. Given an effective precipitation rate  $v_r$ ,  $q_r$  is computed assuming the conservation of surface water along a line running from the drainage divide to the observation point. A rapid decrease of stream power north of the drainage divide, however, is introduced because the rivers are flowing away from a monsoon source area towards the Rub-al-Khali desert in the Arabian interior [W. Thesinger, *Arabian Sands*, 1954]. For those rivers, flow towards an increasingly arid climate is simulated by decreasing the precipitation rate  $v_r$  between 10 km (full rate) and 100 km (zero) north of the escarpment.

In our model, fluvial transport is assumed to be detachment-limited so that river flow is always below critical transport capacity. This ‘undercapacity’ formulation mimics bedrock channel behavior. In this case, the incremental denudation due to fluvial transport is:

$$\frac{dh}{dt} = \frac{q_f^{eqb}}{l_f} = -\frac{K_f q_r}{l_f} \cdot \frac{dh}{dx} \quad (3)$$

where  $l_f$  is the characteristic erosional length scale for fluvial transport (we choose a constant value of 100 km), and is a measure of substrate erodibility. Sediments eroded south of the

drainage divide should be deposited not far from the escarpment, in sedimentary basins such as the Salalah plain or in the submarine depression occurring immediately offshore of the Type 1 scarp. We thus assume that sediments eroded by fluvial transport are deposited along a 20-km long path south of the master normal fault. The total height of erosion  $\Delta H$  at any given node is the sum of the incremental short- and long-range denudations throughout the post-rift time period. At each model step, it is directly compared with the denudation values estimated from reference geological cross-sections (Figs 5 and 6).

### 3.2 Flexural rebound

Flexural rebound of the lithosphere in response to denudation and sedimentation is obtained using the 1D flexure equation:

$$D \cdot \frac{d^4 w}{dx^4} + (\rho_m - \rho_{fill}) g w(x) = q(x) \quad (4)$$

with  $D = \frac{ET_e^3}{12(1-\nu^2)}$  the flexural rigidity, where  $E$  is Young's modulus,  $\nu$  is the Poisson ratio,

$\rho_m$  and  $\rho_{fill}$  are densities of lithospheric mantle and infill of flexural depressions ( $\rho_{fill} = 0$  in the eroded domain). The load  $q(x)$  corresponds either to the height of eroded rocks on the margin (density  $2800 \text{ kg.m}^{-3}$ ), or to the height of deposited sediments in the offshore basins (density  $2400 \text{ kg.m}^{-3}$ , corresponding to an "effective" load density of  $1400 \text{ kg.m}^{-3}$  because sediments deposit under water).  $T_e$  is the effective elastic thickness of the lithosphere and  $w(x)$  is the deflection. High  $T_e$  impedes flexural rebound because the wavelength of the load is always much lower than the characteristic waveband of flexure [Watts, 2001]. Low  $T_e$  will instead result in high-amplitude, short-wavelength uplift increasing topographic slopes and enhancing denudation. Deflection is solved by using a finite-difference approximation of the flexure equation in which the model boundaries are fixed (null deflection).

### 3.3 Model assumptions and limitations

The simple 1D model used implies necessary simplifications and assumptions which we believe are justified by the scale of the experiment and the geological setting. In one-dimensional models, "surface" processes are necessarily restricted to the profile dimension, with the hypothesis that mass transfers in the perpendicular dimension are negligible. Moreover, flexure is also supposed to occur dominantly in the direction of the profile. Given the dominant NW-SE direction of topographic slopes and river channels, the use of one-dimensional models appears a reasonable approximation to the Dhofar setting, at least at the

scale of our experiments (several tens of km). River width is supposed to be constant, which is a great simplification since it does not take into account for widening of fluvial channels downstream. However, we aim at reproducing a mean topography corresponding to the general shape of the escarpment, and not at modeling river profiles. The output topography is an average that corresponds either to numerous tiny channels (close to the escarpment crest for instance) or to few larger rivers (at the profile extremities). Thus, introducing a ‘river width’ parameter is unnecessary in this case.

Based on geologic data (see section 2.1), we assume that the sedimentary sequence is initially 1000 m-thick on average and has been deposited horizontally, so that it was tilted with the topographic surface during rifting and was parallel to the post-rift (i.e., initial) topography. The latter corresponds to a virtual post-rift stage which in reality never existed, since erosion started as soon as vertical motions were large enough to bring rocks to the surface. The initial shape of the unconformity between basement and sediments is not known but the remarkably constant sedimentary thickness, as well as the lack of field evidence for progressive onlapping of the sediments over pre-existing relief support the hypothesis of an originally horizontal unconformity.

We also assume, except in one tested model, that the post-rift topography primarily controlled the drainage network so that the drainage divide initially coincides with the scarp crest. In the model, this is therefore an initial condition and not a boundary condition. During model runs, the drainage divide is therefore free to migrate. Rocks eroded from the drainage divide to the shoreline are deposited seaward of the master normal faults of each escarpment. We simplify the geometry of sediments deposited seaward to 20 km-long rectangular prisms. Sediments routed towards the north effectively exit the model space and have no bearing on the flexural response. The northern area, where true long-term erosion depths of the pre-rift sediment package are negligible (cf. Fig. 5A), provides a convenient natural boundary to the model space.

Finally, a constant post-rift mean sea level is assumed, even though short-term eustatic fluctuations are likely to affect the response of eroding topography over finite time intervals.

### **3.4 Parameters and results**

#### **3.4.1 Modeling of the Type 1 escarpment**

We present in Fig. 7 three different runs that reproduce the topography of the Type 1 scarp equally well if only topography is used as the only constraint (Table 1). This figure

illustrates the issue of equifinality outlined in the introduction, and demonstrate the power of additional independent constraints, such as stratigraphic markers, in improving the quality of an SPM. The best-fitting model involves a mean  $T_e$  of  $7\pm 1$  km and a  $K_d/K_{fr}$  ratio of  $90\pm 10$  (Fig. 7A). According to the restored geologic cross-section, the post-rift (initial topography) is a plateau tilted a few degrees towards the NW and culminating 1500 m a.s.l. against the master fault, which is located at the first slope break in the offshore domain. Eroded sediments deposit in the basin at the foot of the scarp. Unlike the two other model runs presented in Figs. 7B and 7C, this model accurately reproduces the observed denudation and the position of the basal stratigraphic unconformity. A good topographic model can be obtained also without sediment loading and slightly different  $T_e$  and  $K_d/K_{fr}$  ratio values (Fig. 7B). However, the predicted denudation on the north-dipping flank of the plateau is too high, and the virtual unconformity does not pass through the buttes. A different initial topography, with a much higher (2000 m) initial escarpment can provide an equally good topographic model (Fig. 7C) but fails again to reproduce the observed denudation and geometry for the unconformity. In summary, topographic profiles similar to that of the Type 1 scarp can be used to determine climatic (i.e.,  $K_d/K_{fr}$ ) and flexural ( $T_e$ ) parameters, but the quality of fit, and therefore the accuracy of parameter choices, is significantly improved when they are combined with independent stratigraphic data.

The relatively low  $K_d/K_{fr}$  ratio is characteristic of semi-arid climatic conditions [e.g., *Kooi and Beaumont, 1994; Young and Saunders, 1986*]: erosion is dominated by fluvial transport during high-energy seasonal rainstorms, whereas short-scale diffusion due to chemical weathering remains low. The virtual position of the basal unconformity is uplifted above the dissected plain where denudation depths are greater, and plunges down to sea level at the shoreline because of the sediment load in the offshore basin. Maximum denudation occurs 5–10 km seaward of the present-day escarpment, and rapidly decreases northward on the plateau, where sedimentary layers are still well preserved.

### **3.4.2 Modeling of the Type 2 escarpment**

It is hypothesized that the Type 2 scarp has had a more complicated history because of the onset of the monsoon occurring ~15 My ago, and the ‘fog oasis’ setting presented in section 2.2. During the first 10 My (25–15 My ago), i.e. prior to monsoon conditions, we assume that both adjacent fault scarps (proto-Type 1, and proto-Type 2) must have experienced identical climatic conditions (Table 1). Using the same parameters as for the Type 1 scarp ( $K_d/K_{fr} = 90$  and  $T_e = 7$  km), we obtain a very rapid rate of scarp retreat (30 km

in 10 My), which is not in agreement with observations (Fig. 8A). In this first test, eroded sediments deposit in the Salalah plain south of the escarpment. Without sediment loading, the escarpment does not retreat but the basal unconformity is nevertheless uplifted and outcrops at the surface (Fig. 8B). This model appears unrealistic because (i) recent deposits sourced by the rivers flowing seaward across the escarpment occur in the Salalah plain, and (ii) there is no evidence of basement outcrops near the scarp foot.

Following the previously discussed “escarpment retreat” vs. “plateau degradation” processes, it could be argued that the existence of a pre-rift drainage divide located inland of the escarpment would explain the negligible retreat observed at the Type 2 scarp. Fig. 8C shows a model run with the same climatic and flexural parameters as for the Type 1 scarp, but with an antecedent drainage system where the drainage divide is located ~20 km inland of the escarpment. The result is basically the same as for Fig. 8A, because erosion causes a flexural uplift of the southern side of the plateau that rapidly changes the sense of drainage. A similar behavior – i.e., drainage reversal due to the flexural response of the lithosphere – has already been modelled by *Kooi and Beaumont* [1994]. Thus, antecedent drainage is not sufficient to explain the difference in behavior (depth of denudation and rock outcrop pattern) between the Type 1 and Type 2 escarpments.

Impeding scarp retreat without changing climatic parameters can be achieved by increasing  $T_e$ . A high  $T_e$  will dampen the flexural response of the lithosphere to erosion. A good model for the monsoon-free period on the Type 2 scarp, i.e. prior to 15 Ma, is obtained for a minimum  $T_e$  of 15 km (Fig. 8D and Table 1). This model predicts < 5 km of scarp retreat and no uplift of the basal unconformity. Larger  $T_e$  values would produce the same effect, i.e., an almost null flexural uplift, so the value of 15 km is a lower bound for true  $T_e$  along the Type 2 scarp profile.

During the last 15 Ma of the model corresponding to the monsoon period, climatic parameters are modified to simulate a more humid climate (Table 1). The best-fitting model involves a high  $K_d/K_{\nu_r}$  ratio of 1000, which means that short-scale diffusion processes due to enhanced rock weathering dominate over fluvial transport (Fig. 9A). This parameterization is justified by the fact that, even though the Type 1 and Type 2 scarps have probably experienced similar rainfall conditions during times since 15 Ma when the ITCZ has been positioned well to the north of its current mean position (cf. section 2.2 and Fig. 4A), scarp 2 in situations such as today (cf. Figs 3 and 4B) receives more precipitation than scarp 1. Although this occurs mostly as fog, we assume this nevertheless entails significant cumulative consequences in terms of rock weathering and soil-forming potential, hence the lush

vegetation observed in the Salalah fog oasis. Eroding landscapes dominated by regolith formation are commonly dominated in SPMs by diffusional processes. Consequently, because of the relatively high  $T_e$ , the scarp crest is smoothed *in situ* and its retreat rate is low. The predicted basal unconformity remains buried but approaches the surface close to the scarp foot. This matches the observed stratigraphy. Diffusion processes are also responsible for producing the recent sedimentary deposits that currently mask the original fault trace, also in agreement with geologic observations [Platel *et al.*, 1992].

Two other tests were performed in order to determine how sensitive the topography of the Type 2 scarp has been to the onset of the monsoon ca. 15 My ago, and whether it can, instead, be modeled using constant climatic parameters throughout its 25 My history. When “monsoon” climatic parameters (as depicted in Fig. 4A) act during the entire post-breakup period (25 My), the escarpment slopes are smoothed and the drainage divide progressively retreats (Fig. 9B). The predicted topography and denudation provide good fits to observations, except inboard of the escarpment where the predicted denudation is slightly underestimated. Finally, with arid (entirely monsoon-free) climatic parameters acting during 25 My, the modeled topography and denudation do not match the observations at all, since the amounts of predicted retreat and denudation at the escarpment front are much too large (Fig. 9C).

## 4 Discussion-Conclusion

The area presented in this study is ideally suited to experimenting with flexural model parameterizations in a real-world setting because the lithology and stratigraphy at the Type 1 and Type 2 escarpments are known, and these provide robust constraints in addition to the topography. Models in the past have usually tested the influence of initial topography, lithology, interior catchment base-level lowering, climate change and lithospheric rigidity as parameters controlling margin evolution and singularity [e.g. *Beaumont et al.*, 1994; *Gilchrist et al.*, 1994]. Our results suggest that the last two parameters, namely climate and flexural rigidity, are both responsible for the contrasting escarpment morphologies flanking the Gulf of Aden. However, we show that  $T_e$  controls first-order contrasts relating to large-scale scarp retreat and flexural rebound, whereas climatic differences principally affect scarp morphology (principally profile form).

The formation of the steep and retreating Type 1 scarp reflects a semi-arid climate and a high component of flexural rebound of the lithosphere in response to erosion. Deformation of the basal unconformity shows that scarp uplift is balanced by a downward flexure of the lithosphere due to sedimentary loading in the offshore basin close to the main normal fault.

Erosion depths calculated by the forward 1-D model for the Type 1 scarp are in good agreement with the values obtained from geological cross-sections and independent thermochronologic analyses [Gunnell *et al.*, in review]. On the other hand, the Type 2 scarp results from predominantly short-range erosion processes more typical of humid climatic conditions, associated with a  $T_e$  value at least double that of the Type 1 scarp. This prevents scarp uplift and retreat, so that the Salalah escarpment is essentially still a fault scarp, which has undergone minor morphologic alterations in an essentially low-energy, semiarid but seasonally moist climate. It is therefore confirmed that the monsoon has, on average, been an influential long-term agent in shaping the Dhofar escarpments despite the present-day dominant impression of aridity. In conclusion, it remains difficult to assess purely on the basis of morphologic criteria whether the onset of humid monsoon conditions could have started even earlier than 15 My ago. A slightly better fit to observations and the consistency with *Prell et al.* [1990] analyses of ODP Leg 117 lead us to prefer the 15 My model (Fig. 9A) over any other (Fig. 9B and 9C). The lateral transition from the Type 1 to Type 2 scarps is very rapid and coincides with a change in the cumulative effect of long-term summer monsoon impacts. However, it appears predominantly due to margin segmentation (Fig. 2). The master normal faults associated with those escarpments are arranged in a left-stepping en échelon system, whereas the tilted blocks offshore, including the continent–ocean boundary, display left-lateral offsets due to the presence of several transform faults [*d’Acremont et al.*, 2005]. Whether this geometry is a consequence of rift processes, or an older inherited feature that has controlled rift segmentation, is difficult to assess. This segmentation is also reflected in the lateral variations of  $T_e$ , which changes from 7 to  $\geq 15$  km from scarp 1 to scarp 2. Both values are low for a continental lithosphere [e.g., *Watts and Burov*, 2003], and much lower than expected for the stable core of the Arabian plate [*Cloetingh et al.*, 1995; *van der Beek et al.*, 1994]. It seems thus that the Oman lithosphere in Dhofar has been significantly weakened during rifting, and/or after it because erosion and sedimentation displace loads on the lithosphere and have an influence on its strength [*Burov and Cloetingh*, 1997]. Similarly low  $T_e$  values are also required to explain escarpment evolution along the southeast African [*van der Beek et al.*, 2002] and southeast Australian [*Braun and van der Beek*, 2004] margins, where required best-fit values are 10 km and 7 km, respectively.

Finally, our models suggest that sedimentary loads at the foot of a scarp can have a significant effect on scarp evolution, as already pointed out by *Pazzaglia and Gardner* [1994]. This parameter is generally omitted in such models [e.g., *Kooi and Beaumont*, 1994; *van der Beek et al.*, 2002] because it is difficult to constrain unless detailed offshore records are

available, and because the sedimentary load is assumed to be deposited far from the escarpment. At the Oman margin, the escarpments are young and located very close to two major basins, which are likely to trap a large part of the incoming sedimentary flux. We demonstrate that the flexural load caused by the deposition (or non-deposition) of eroded sediments has a significant influence on the flexural behavior of the escarpment, and thus on its evolution, than previously considered by most long-term passive margin evolution models.

**Acknowledgments.** Many thanks to Esther Bordet who initiated this work. Constructive reviews by H. Sinclair, A. Matmon and G. Rosenbaum (Associate Editor) were greatly appreciated.

## References.

- Bellahsen, N., M. Fournier, E. d'Acremont, S. Leroy, and J.-M. Daniel (2006), Fault reactivation and rift localization: The northeastern Gulf of Aden margin, *Tectonics*, 25, doi : 10.1029/2004TC001747.
- Braun, J., and van der Beek, P. (2004), Evolution of passive margin escarpments: what can we learn from low-temperature thermochronology? *Journal of Geophysical Research*, v. 109, F04009, doi: 10.1029/2004JF000147.
- Burov, E.B. and S.A.P.L. Cloetingh (1997), Erosion and rift dynamics: new thermomechanical aspects of post-rift evolution of extensional basins, *Earth Planet. Sci. Lett.*, 150, 7-26.
- Cloetingh, S., van Wees, J.D., van der Beek, P.A. and G. Spadini (1995), Role of prerift rheology in kinematics of extensional basin formation: constraints from thermomechanical models of Mediterranean and intracratonic basins, *Mar. Geol.* 12, 793-807.
- d'Acremont, E., Leroy, S., Beslier, M.-O., Bellahsen, N., Fournier, M., Robin, C., Maia, M., and P. Gente (2005), Structure and evolution of the eastern Gulf of Aden conjugate margins from seismic reflection data. *Geophys. J. Int.* 160, 869–890.
- Fleitmann, D., Burns, S. J., Mudelsee, M., Neff, U., Kramers, J., Mangini, A., and A. Matter (2003), Holocene forcing of the Indian monsoon recorded in a stalagmite from southern Oman, *Science*, 300, 1737–1739.
- Fournier, M., P. Patriat, and S. Leroy (2001), Reappraisal of the Arabia-India-Somalia triple junction kinematics, *Earth Planet. Sci. Lett.*, 184, 103–114.
- Fournier, M., N. Bellahsen, O. Fabbri, and Y. Gunnell (2004), Oblique rifting and segmentation of the NE Gulf of Aden passive margin, *Geochem. Geophys. Geosyst.*, 5, Q11005, doi:10.1029/2004GC000731.
- Gilchrist, A. R., Kooi, H. and C. Beaumont (1994), The post-Gondwana geomorphic evolution of southwestern Africa: Implications for the controls on landscape development from observations and numerical experiments, *J. Geophys. Res.*, 99, 12,211-12,228.
- Gilchrist, A. R., and M.A. Summerfield (1990), Differential denudation and flexural isostasy in formation of rifted-margin upwarps, *Nature*, 346, 739-742.
- Gunnell, Y. (1998), Passive margin uplifts and their influence on climatic change and weathering patterns of tropical shield regions. *Global and Planetary Change*, 18, 47-57.
- Gunnell, Y., Carter, A., Petit, C., and M. Fournier (2006), Constraints on rift-shoulder downwarp in southern Oman using apatite fission-track analysis, (U–Th)/He dating, and stratigraphy, *Geology*, in review.
- Gunnell, Y. and L. Fleitout (1998), Shoulder uplift of the Western Ghats passive margin, India - a flexural model. *Earth Surface Processes and Landforms* , 23, 391-404.
- Huchon, P., and K. Khanbari (2003), Rotation of the syn-rift stress field of the northern Gulf of Aden margin, Yemen, *Tectonophysics*, 364, 147–166.
- Hughes, G. W., O. Varol, and Z. R. Beydoun (1991), Evidence for middle Oligocene rifting of the Gulf of Aden and for late Oligocene rifting of the southern Red Sea, *Mar. Petrol. Geol.*, 8, 354-358.
- Jestin, F., P. Huchon, and J. M. Gaulier (1994), The Somalia plate and the East African rift system: Present-day kinematics, *Geophys. J. Int.*, 116, 637–654.
- Jung, S. J. A., Ivanova, E., Reichart, G. J., Davies, G. R., Ganssen, G., Kroon, D., and J.E. van Hinte (2002), Centennial-millennial-scale monsoon variations off Somalia over the last 35 ka, Clift, P. D., Kroon, D., Gaedicke, C. and Craig, J. (eds), *The Tectonic and Climatic evolution of the Arabian Sea region*, *Geol. Soc. London Spec. Publ.*, 195, 341-352.

- Kooi, H., and C. Beaumont (1994), Escarpment evolution on high-elevation rifted margins: insights derived from a surface processes model that combines diffusion, advection and reaction, *J. Geophys. Res.*, *99*, 12,191-12,210.
- Lepvrier, C., Fournier, M., Bérard, T., and J. Roger (2002) Cenozoic extension in coastal Dhofar (southern Oman): implications on the oblique rifting on the Gulf of Aden, *Tectonophysics*, *357*, 279-293.
- Leroy, S., P. Gente, M. Fournier, E. d'Acremont, N. Bellahsen, M.-O. Beslier, P. Patriat, M. Maia, A. Blais, J. Perrot, A. Al-Kathiri, S. Merkouriev, P.-Y. Ruellan, J.-M. Fleury, C. Lepvrier, and P. Huchon (2004), From rifting to spreading in the eastern Gulf of Aden: a geophysical survey of a young oceanic basin from margin to margin, *Terra Nova*, *16*, 185-192.
- Mercogli, I., Briner, A.P., Frei, R., Schönberg, R., Nægler, T.F., Kramers, J. and T. Peters (2006), Lithostratigraphy and geochronology of the Neoproterozoic basement of Salalah, Dhofar, Sultanate of Oman, *Precambrian Res.* *145*, 182-206.
- Pazzaglia, F. J, and Gardner, T.W. (1994), Late Cenozoic flexural deformation of the middle U.S. Atlantic passive margin, *J. Geophys. Res.*, *99*, 12,143-12,157.
- Platel, J.-P. and J. Roger (1989), Evolution géodynamique du Dhofar (Sultanat d'Oman) pendant le Crétacé et le Tertiaire en relation avec l'ouverture du golfe d'Aden. *Bull. Soc. Géol. France*, *2*, 253-263.
- Platel, J.P., Roger, J., Peters T.J., Mercogli, I, Kramers, J.D. and J. Le Métour (1992), Geological map of Salalah, Sultanate of Oman, sheet NE 40-09, scale 1:250,000, *Oman Ministry of Petroleum and Minerals*, Directorate General of Minerals.
- Prell, W. L. and shipboard party of ODP Leg 117 (1990), Neogene tectonics and sedimentation of the SE Oman continental margin: results from ODP Leg 117, Robertson, A. H. F., Searle, M. P. and Ries, A. C. (eds), "The Geology and Tectonics of the Oman region", *Geol. Soc. Spec. Publ.* *49*, 745-758.
- Rodriguez, E., C.S. Morris, J.E. Belz, E.C. Chapin, J.M. Martin, W. Daffer, and S. Hensley (2005), An assessment of the SRTM topographic products, Technical Report JPL D-31639, *Jet Propulsion Laboratory*, Pasadena, California, 143 pp.
- Roger, J., J.-P. Platel, C. Cavelier and C. Bourdillon-de-Grisac (1989), Données nouvelles sur la stratigraphie et l'histoire géologique du Dhofar (Sultanat d'Oman). *Bull. Soc. Géol. France*, *2*, 265-277.
- Sale, J. B. (1980), The environment of the Mountain Region of Dhofar. In: Shaw Reade S. N., Sale, J. B., Gallagher, M. D., and Daly, R. H. (Eds.), The scientific results of the Oman flora and fauna survey 1977 (Dhofar), *Journal of Oman Studies*, Special Report No. 2. Office of the Government Advisor for Conservation of the Environment; pp. 17-23.
- Sirocko, F., Sarnthein, M., Lange, H. and H. Erlenkeuser (1991), Atmospheric summer circulation and coastal upwelling in the Arabian Sea during the Holocene and the Last Glaciation. *Quaternary Res.*, *36*, 72-93.
- Smith, W.H.F. and D.T. Sandwell (1997), Global seafloor topography from satellite altimetry and ship depth soundings, *Science*, *277*, 1957-1962.
- Ten Brink, U. and T. Stern (1992), Rift flank uplifts and hinterland basins: comparison of the Transantarctic Mountains with the Great Escarpment of southern Africa, *J. Geophys. Res.*, *97*, 569-585.
- van der Beek, P.A., Cloetingh, S.A.P.L., and P.A.M. Andriessen (1994), Mechanisms of extensional basin formation and vertical motions at rift flanks: constraints from tectonic modeling and fission track thermochronology, *Earth Planet. Sci. Lett.*, *121*, 417-433.

- van der Beek, P.A., Andriessen, P.A.M. and S.A.P.L. Cloetingh (1995), Morphotectonic evolution of rifted continental margins: Inferences from a coupled tectonic-surface processes model and fission track thermochronology. *Tectonics*, 14, 406-421.
- van der Beek, P., Summerfield, M. A., Braun, J., Brown, R. W., and A. Fleming (2002), Modeling postbreakup landscape development and denudational history across the southeast African (Drakensberg Escarpment) margin, *J. Geophys. Res.*, 107, doi:10.1029/2001JB000744.
- Watchorn, F., G.J. Nichols and D.W.J. Bosence (1998), Rift-related sedimentation and stratigraphy, southern Yemen (Gulf of Aden). In: Sedimentation and Tectonics of Rift Basins: Red Sea- Gulf of Aden. Edited by B.H. Purser and D.W.J. Bosence, Chapman & Hall, London, 165-191.
- Watts, A.B. (2001), Isostasy and Flexure of the Lithosphere. Cambridge University Press, Cambridge, 478 p.
- Watts, A.B., and E.B. Burov (2003), Lithospheric strength and its relationship to the elastic and seismogenic layer thickness, *Earth Planet. Sci. Lett.*, 213, 113-131.
- Weissel, J.K. and G.D. Karner (1989), Flexural uplift of rift flanks due to mechanical unloading of the lithosphere during extension, *J. Geophys. Res.* 94, 13,919-13,950.
- Young, A., and Saunders, I. (1986), Rates of surface processes and denudation, A. D. Abrahams (eds)., in Hillslope processes, Allen and Unwin, Boston, Mass., 3-27.

## Figure Captions.

Fig. 1. General setting of the study region. Open dots are earthquake epicentres, and solid arrows reflect relative plate motions between India, Arabia and Somalia [Fournier *et al.*, 2001].

Fig. 2. Topography, bathymetry and main faults in Dhofar. Topography comes from the global SRTM model [Rodriguez *et al.*, 2005]. Bathymetry is a compilation of worldwide data [Smith and Sandwell, 1997] and of seabeam data acquired during the ENCENS-SHEBA cruise [Leroy *et al.*, 2004]. AA' and BB' lines locate the topographic profiles modeled in this study.

Fig. 3. A- Drainage network (thin solid lines), faults (thick lines), main drainage divide (thick dashed line) and directions of drainage (arrows) in Dhofar. Source: Digital Chart of the World (DCW). B- Landsat image of the Dhofar region in summer. Green patches correspond to natural vegetation growth due to increasing humidity. Broken lines labelled 1 and 2 show the position of the Google Earth panoramas presented in Figs. 4 and 5. Arrows show the dominant direction of monsoon winds.

Fig. 4. Variable impact of monsoon winds on precipitations depending on the position of the ITCZ. A: a low-latitude ITCZ causes moist monsoon air to flow nearly parallel to the coast and to generate only low-altitude fog in the Jabal Qara re-entrant; B: a higher-latitude ITCZ causes monsoon wind to penetrate deeper into the Arabian continent and strike the entire Dhofar margin perpendicularly while generating higher rainfall.

Fig. 5. A- Google Earth view of the Type 1 scarp (Jabal Samhan) towards the NE (left panel), and its interpretation (right panel). See Fig. 3 for the panorama location. B- Close-up view (see location on Figure 5A) . C- Geologic cross-section (top panel) with denudation estimates (circled numbers) along the AA' profile [surface geology after Platel *et al.*, 1992], and estimated initial topography (bottom panel).

Fig. 6. Same legend as for Fig. 5, for the Type 2 scarp (Jabal Qara).

Fig. 7. Three forward models of the Type 1 scarp. These predict approximately the same topographic output, but different denudation depths and positions of the basal unconformity (see text for explanations).

Fig. 8. Forward models of the Type 2 scarp during the first, monsoon-free, 10 My period. A- Same parameters as for Type 1 scarp in Fig. 7A; B- Same parameters as A but without sedimentary loading in the Salalah basin; C- Same parameters as A but with antecedent drainage. D- Same parameter as A but with higher  $T_e$  (15 km).

Fig. 9. Forward model of the Type 2 scarp during the last 15 My monsoon period. A- 15 My monsoon period (continuing after model 8D); B- Hypothetical 25 My monsoon period (i.e., over the entire model duration); C- Hypothetical 25 Ma monsoon-free period (i.e., same climatic parameters as for the Type 1 scarp during 25 My).

Figure 1

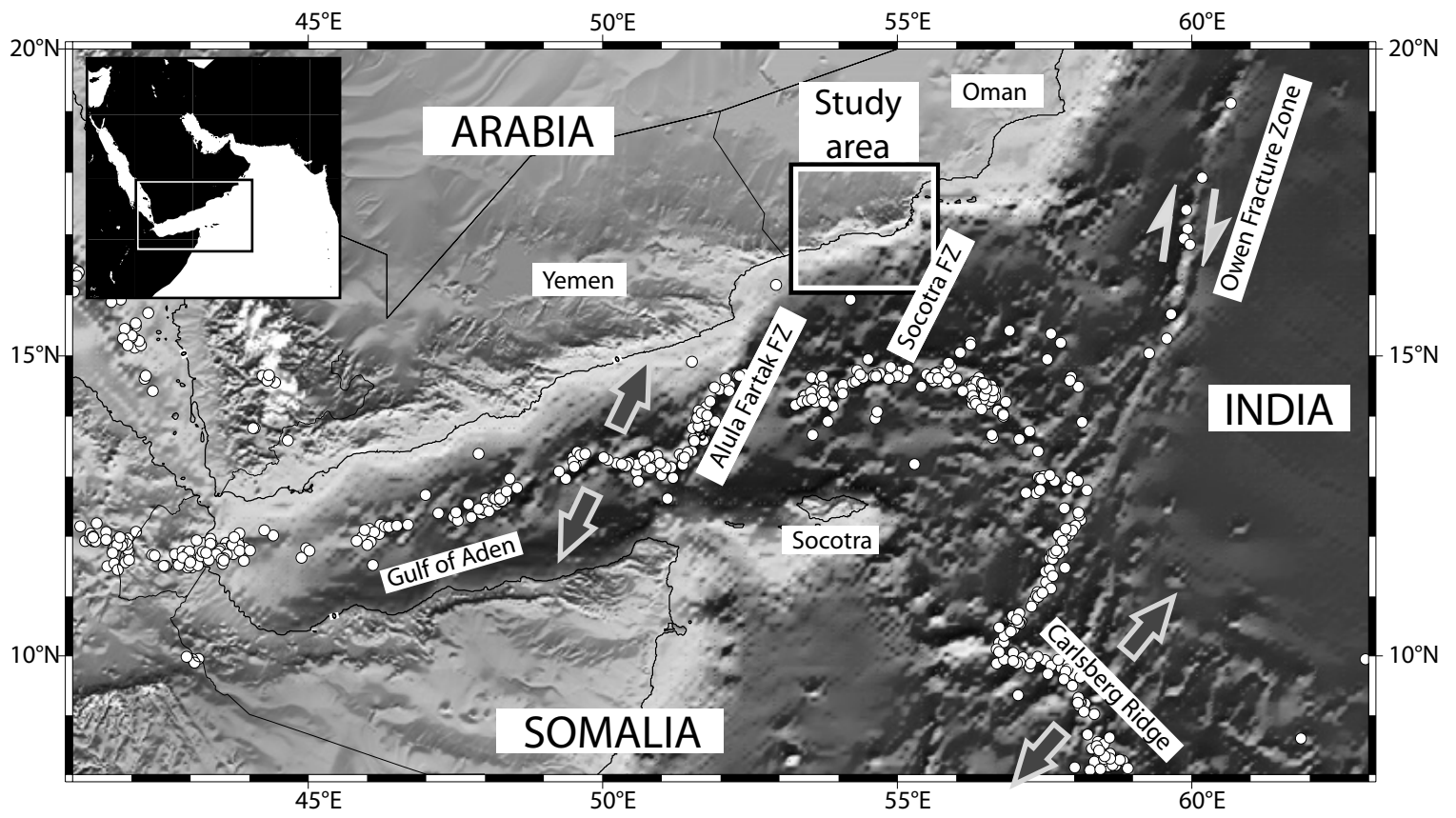


Figure 2

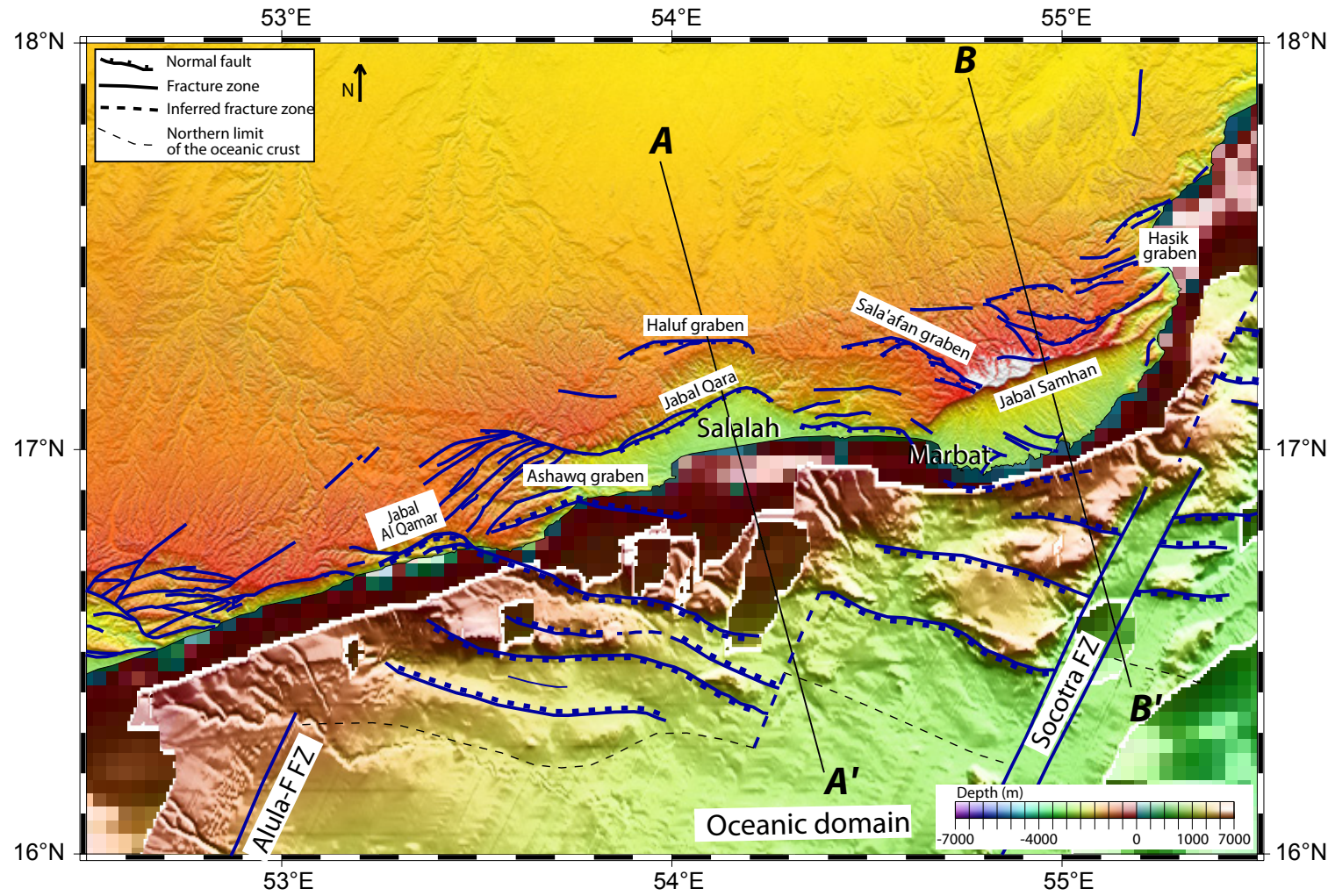


Figure 3

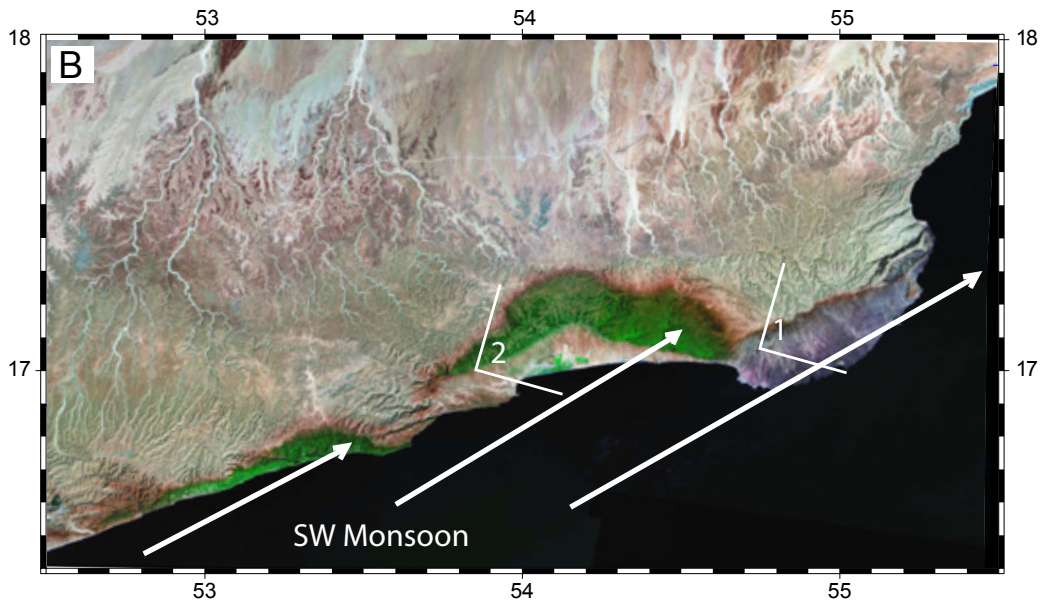
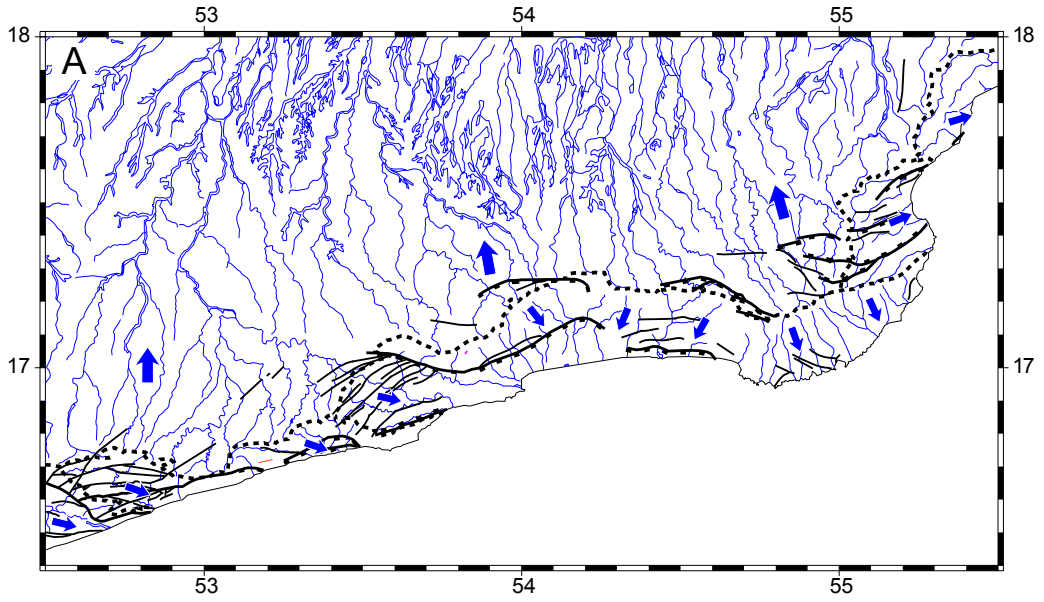


Figure 4

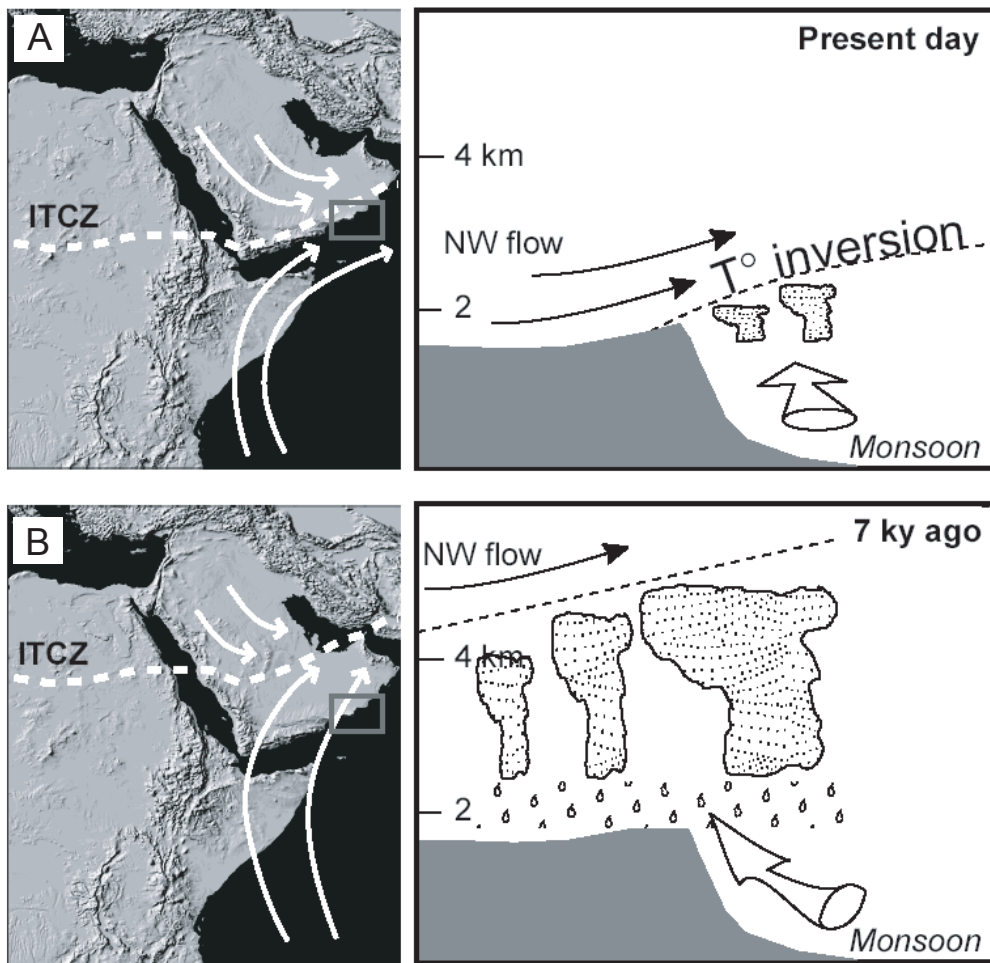
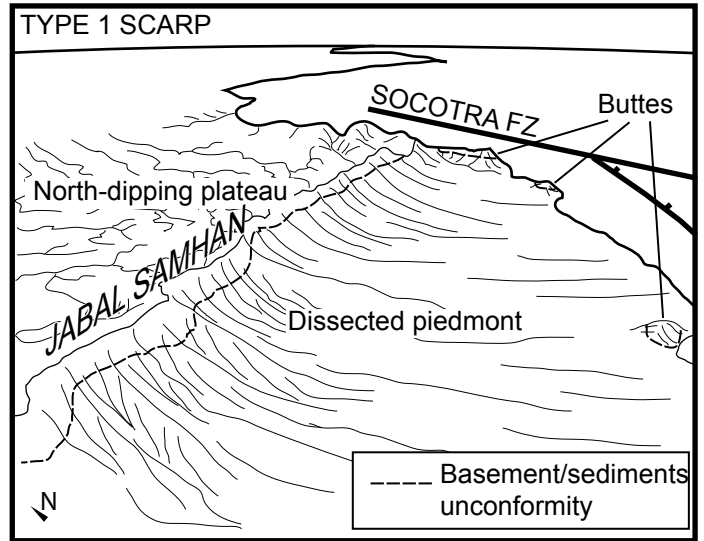
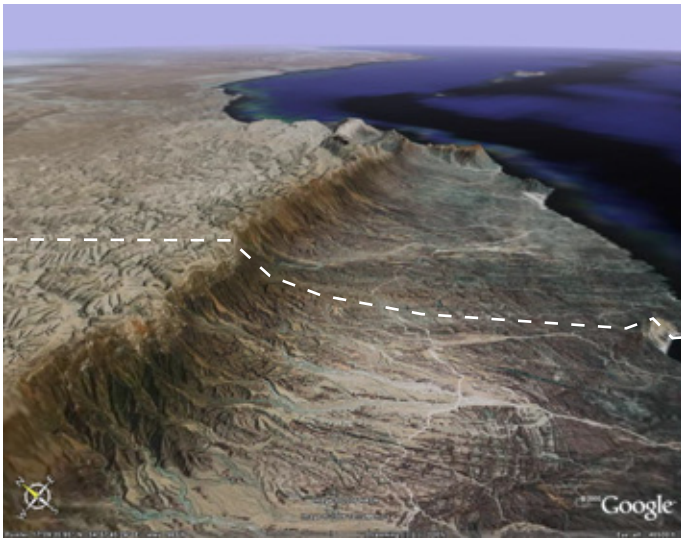


Figure 5

A - Panoramic view



B - Geologic cross-section

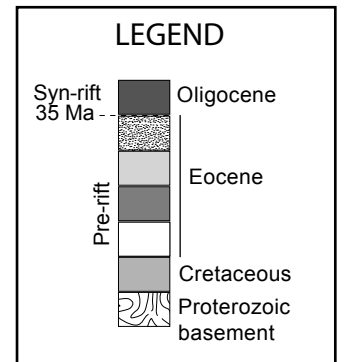
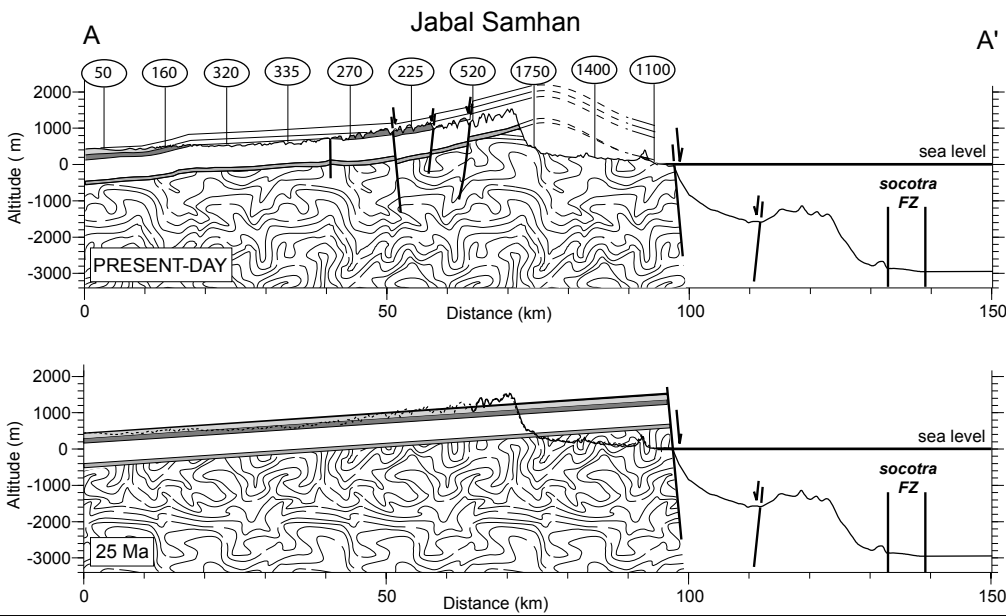
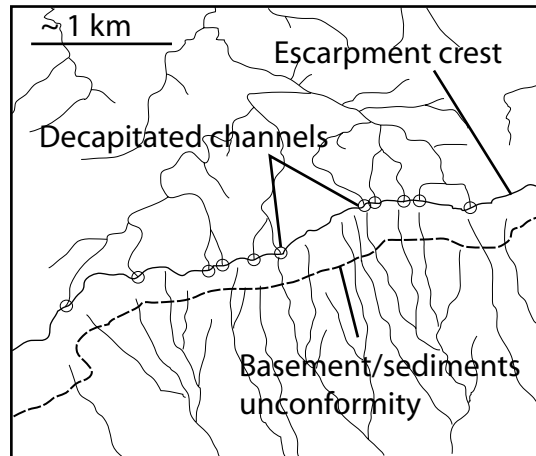
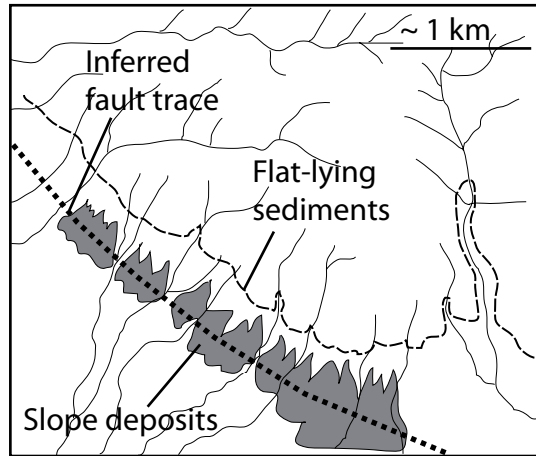


Figure 6

A-TYPE 1 SCARP



B-TYPE 2 SCARP



B - Geologic cross-section

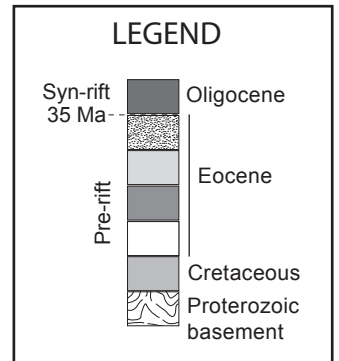
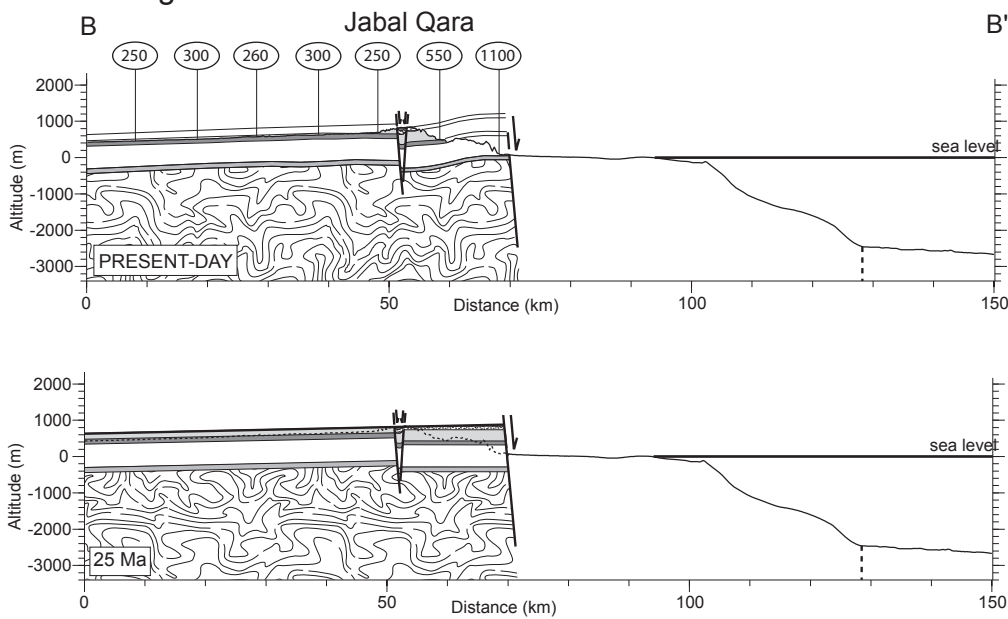


Figure 7

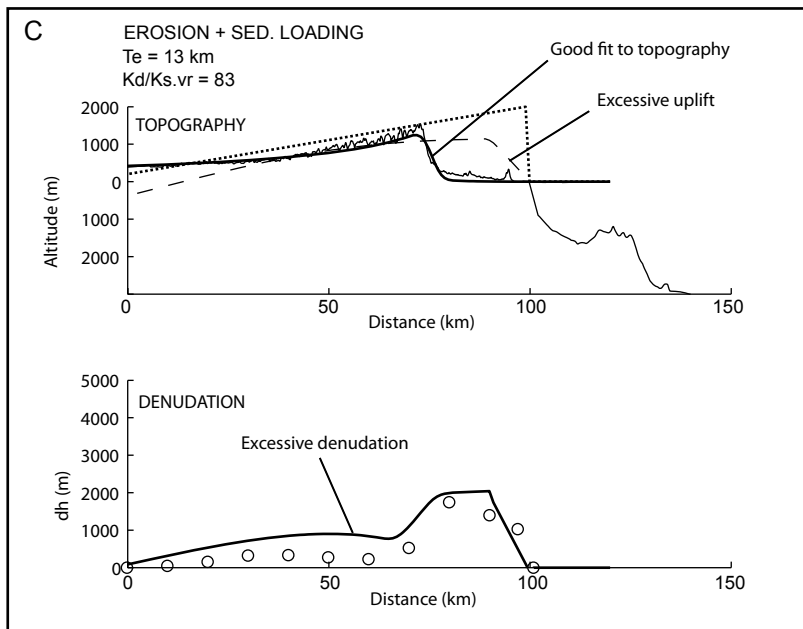
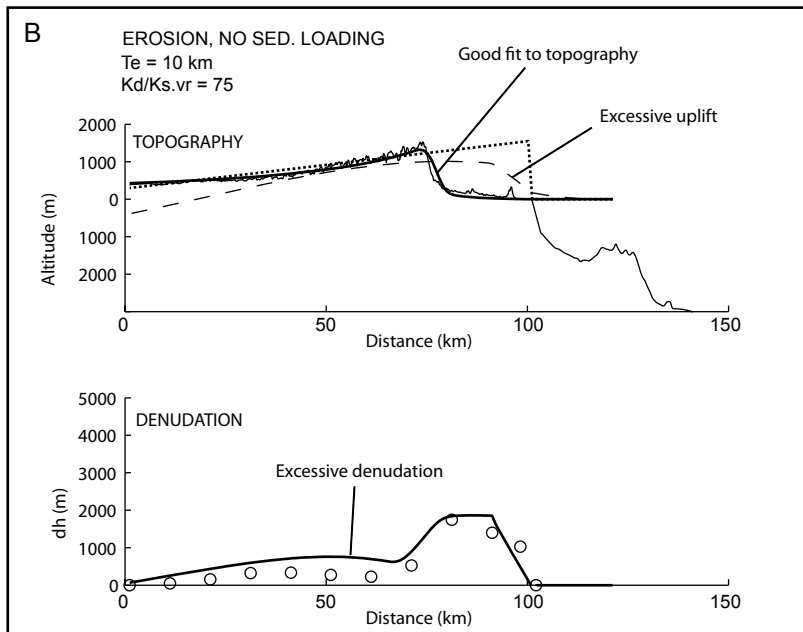
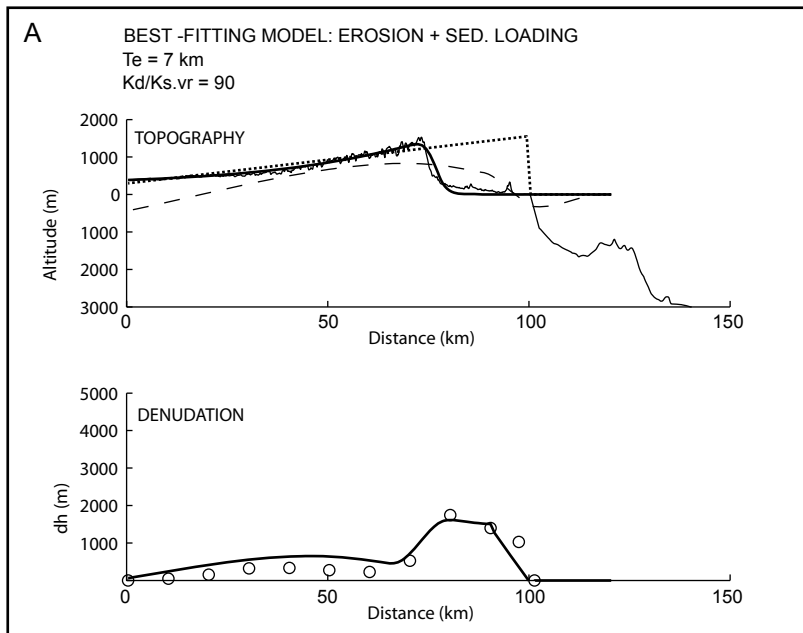


Figure 8

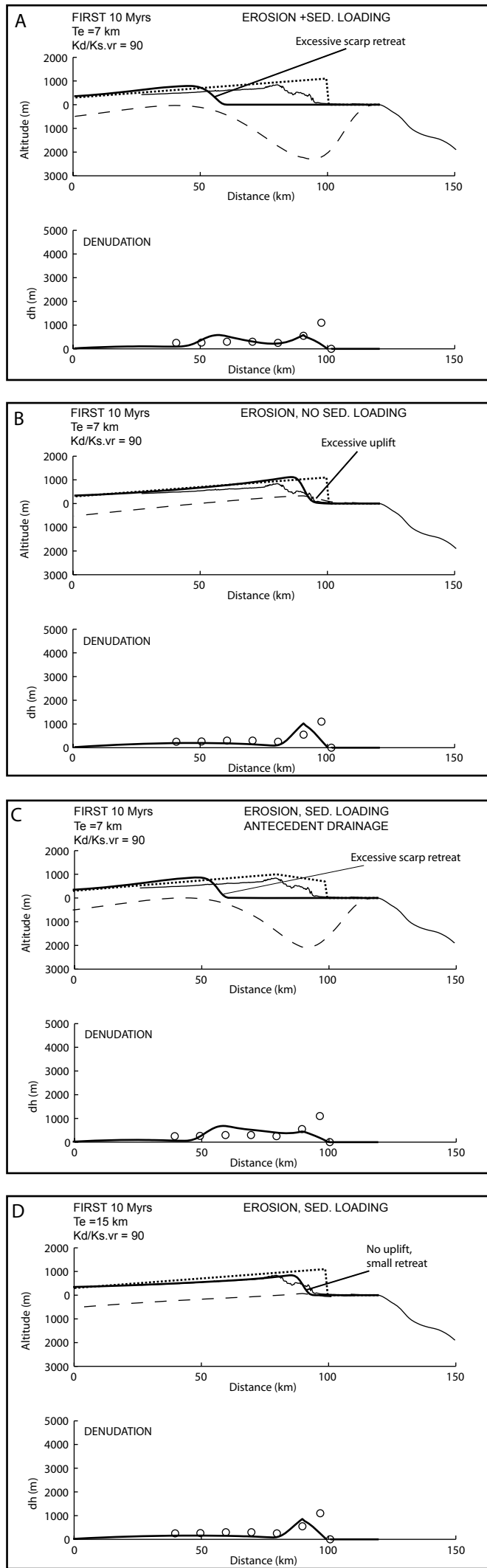


Figure 9

